

**A98-30841****AIAA-98-2267**

## Numerical Solution of Acoustic Propagation Problems Using linearized Euler's Equations\*

Christophe Bailly<sup>†</sup> and Daniel Juvé<sup>‡</sup>Laboratoire de Mécanique des Fluides et d'Acoustique  
Ecole Centrale de Lyon & UMR CNRS 5509  
BP 163, 69131 Ecully cedex, France.**Abstract**

The goal of this work is to study some numerical solutions of acoustic propagation problems using linearized Euler's equations. The two-dimensional Euler's equations are linearized around a stationary mean flow. The solution is obtained by using a dispersion-relation-preserving scheme in space, combined with a fourth-order Runge-Kutta algorithm in time. This numerical integration leads to very good results in terms of accuracy, stability and low storage. The radiation of a source in a subsonic and supersonic uniform mean flow is investigated. The numerical estimates are shown to be in excellent agreement with the analytical solutions. Next, a typical problem in jet noise is considered, the propagation of acoustic waves in a sheared mean flow, and the numerical solution compares favorably with ray tracing. The final goal of this work is to improve and to validate the Stochastic Noise Generation and Radiation (SNGR) model. In this model, the turbulent velocity field is modeled by a sum of random Fourier modes through a source term in the linearized Euler's equations. The implementation of acoustic sources in the linearized Euler's equations is thus an important point. This is discussed with emphasis on the ability of the method to describe correctly the multipolar structure of aeroacoustic sources. Finally, a nonlinear formulation of Euler's equations is solved in order to limit the growth of instability waves excited by the acoustic source terms.

**1. Introduction**

Sound generation and propagation in a turbulent flow is a very difficult numerical problem.<sup>1,2</sup> Lighthill's analogy is one of the classical approaches

to solve it. Lighthill's wave equation<sup>3</sup> is written as:

$$\frac{\partial^2 \rho'}{\partial t^2} - c_o^2 \nabla^2 \rho' = \frac{\partial^2 T_{ij}}{\partial x_i \partial x_j} \quad (1)$$

where  $T_{ij} \approx \rho u_i u_j$ . This wave equation is exact only for an homogeneous medium at rest. The Green function is required in order to obtain an integral formulation. Hence, only simple geometric configurations can be studied when the turbulent velocity field is known or modeled. The case of the noise generated in a duct obstructed by a diaphragm is one of the most complex geometry investigated in the literature.<sup>4</sup> Furthermore, refraction effects are not taken into account with (1).

The linearized Euler's equations are an alternative approach in computational aeroacoustics. Euler's equations are linearized around a stationary mean flow, previously calculated by solving the Reynolds-averaged Navier-Stokes equations. Then, a turbulent source term is introduced in the linearized equations. A first formulation has been used to calculate a subsonic jet noise in the axisymmetric case.<sup>5-7</sup> In this Stochastic Noise Generation and Radiation model, the turbulent velocity field was modeled by a sum of random Fourier modes.

The goal of this study is to improve this approach using a new algorithm, described in section 2. In addition, the implementation of source terms in the linearized Euler's equation is investigated. The case of source radiation in a subsonic and a supersonic uniform mean flow is studied in section 3. The analytical solution is known for these cases. Section 4 deals with propagation in a sheared mean flow, and the numerical solution is compared to ray-tracing. It is shown in section 5 that the multipolar feature of a source distribution is preserved in solving linearized Euler's equations.<sup>8</sup> Finally, a nonlinear formulation is developed in order to limit the growth of instability waves, which are also supported by the linearized

\*Copyright © 1998 by the Confederation of European Aerospace Societies, All rights reserved.

<sup>†</sup>Assistant Professor, Member AIAA

<sup>‡</sup>Professor, Member AIAA

equations.

## 2. Numerical Algorithm

### 2.1 Governing equations

The density  $\rho'$ , the velocity  $\mathbf{u}'$  and the pressure  $p'$  designate small perturbations superimposed on a mean flow of density  $\rho_o$ , velocity  $\mathbf{u}_o$  and pressure  $p_o$ .  $\gamma$  designates the ratio of specific heats, and is taken as  $\gamma = 1.4$  for air. The Euler's equation linearized around a stationary mean flow, can be written as:

$$\frac{\partial \mathbf{U}}{\partial t} + \frac{\partial \mathbf{E}}{\partial x} + \frac{\partial \mathbf{F}}{\partial y} + \mathbf{H} = \mathbf{S} \quad (2)$$

where the unknown vector  $\mathbf{U}$  and the flux vectors  $\mathbf{E}$  and  $\mathbf{F}$  are given, for the two-dimensional case, by:

$$\mathbf{U} = \begin{pmatrix} \rho' \\ \rho_o u' \\ \rho_o v' \\ p' \end{pmatrix} \quad \mathbf{E} = \begin{pmatrix} \rho' u_o + \rho_o u' \\ u_o \rho_o u' + p' \\ u_o \rho_o v' \\ u_o p' + \gamma p_o u' \end{pmatrix}$$

and

$$\mathbf{F} = \begin{pmatrix} \rho' v_o + \rho_o v' \\ v_o \rho_o u' \\ v_o \rho_o v' + p' \\ v_o p' + \gamma p_o v' \end{pmatrix}$$

The vector  $\mathbf{H}$  contains mean flow gradient terms, which are equal to zero when the mean flow is uniform:

$$\mathbf{H} = \begin{pmatrix} 0 \\ (\rho_o u' + \rho' u_o) \frac{\partial u_o}{\partial x} + (\rho_o v' + \rho' v_o) \frac{\partial u_o}{\partial y} \\ (\rho_o u' + \rho' u_o) \frac{\partial v_o}{\partial x} + (\rho_o v' + \rho' v_o) \frac{\partial v_o}{\partial y} \\ (\gamma - 1) \left( p' \nabla \cdot \mathbf{u}_o - u' \frac{\partial p_o}{\partial x} - v' \frac{\partial p_o}{\partial y} \right) \end{pmatrix}$$

The vector  $\mathbf{S}$  represents possible unsteady sources in the flow.

### 2.2 Numerical Scheme

All the variables are nondimensionalized with the following scales:  $\Delta x$  for the length scale,  $c_o$  for the velocity scale,  $\Delta x/c_o$  for the time scale,  $\rho_o$  for the density scale and  $\rho_o c_o^2$  for the pressure scale, where  $\Delta x = \Delta y$  is the mesh step size and  $c_o$  the ambient speed of sound. The 7-point stencil, dispersion preserving (DRP) scheme of Tam & Webb<sup>9</sup> is used for the spatial flux derivations of the system (2):

$$\frac{\partial \mathbf{U}_i}{\partial t} = - \sum_{l=-3}^3 a_l (\mathbf{E}_{i+l,j} + \mathbf{F}_{i,j+l}) - \mathbf{H}_{i,j} + \mathbf{S}_{i,j}$$

These authors chose the coefficients<sup>9,1</sup>  $a_l$  of their spatial discretization by requiring that the wave number  $\bar{k}$ , provided by the finite difference scheme be a close approximation to the expected wave number. This optimized fourth-order scheme is better than a non-optimized sixth-order scheme using the same 7-point stencil. Using the criterion  $|k - \bar{k}| < 0.005$ , the resolution for these standard central finite differences (CFD) in terms of points per wavelength is:

CFD second-order	$k \leq 0.30$	$\lambda \geq 21.3$
CFD fourth-order	$k \leq 0.67$	$\lambda \geq 9.3$
CFD sixth-order	$k \leq 0.96$	$\lambda \geq 6.6$
7-pt DRP scheme	$k \leq 1.16$	$\lambda \geq 5.4$

In some cases it is necessary to remove spurious numerical oscillations due to non linearities or mismatches with the boundary conditions or the initial conditions. These short waves can be filtered by an artificial selective damping proposed by Tam & Shen.<sup>10</sup> The damping terms are added to the right side of the system (2) to obtain:

$$\mathbf{D}_{i,j} = - \frac{1}{R_s} \sum_{l=-3}^3 d_l (\mathbf{U}_{i+l,j} + \mathbf{U}_{i,j+l})$$

where  $R_s$  is the mesh Reynolds number, which is usually taken in the interval [5 ; 10]. The notation  $R_s = \infty$  designates a calculation without artificial damping. The coefficients<sup>10,1</sup>  $d_j$  are chosen to damp only the short waves and not the long waves corresponding to an accurate resolution of the DRP scheme. The Fourier transform of the damping function collapses to the Gaussian function:

$$\exp \left[ - \ln 2 ((k\Delta x - \pi) / \sigma)^2 \right]$$

with a half-width  $\sigma = 0.2\pi$  for the linearized Euler's equation. The time integration is performed by through a four step Runge-Kutta algorithm for its high stability limit and its low storage requirement. The solution at time step  $n + 1$  is obtained by the following algorithm:

$$\begin{aligned} \mathbf{U}_i^1 &= \mathbf{U}_i^n + \alpha_1 \Delta t \mathbf{K}_i^n \\ \mathbf{U}_i^2 &= \mathbf{U}_i^n + \alpha_2 \Delta t \mathbf{K}_i^1 \\ \mathbf{U}_i^3 &= \mathbf{U}_i^n + \alpha_3 \Delta t \mathbf{K}_i^2 \\ \mathbf{U}_i^{n+1} &= \mathbf{U}_i^n + \alpha_4 \Delta t (\mathbf{K}_i^3 + \mathbf{D}_i^n) \end{aligned} \quad (3)$$

with:

$$\mathbf{K}_{i,j}^k = - \sum_{l=-3}^3 a_l (\mathbf{E}_{i+l,j}^k + \mathbf{F}_{i,j+l}^k) - \mathbf{H}_{i,j}^k + \mathbf{S}_{i,j}^k$$

$$\mathbf{D}_{i,j}^n = -\frac{1}{R_s} \sum_{l=-3}^3 d_l (\mathbf{U}_{i+1,j}^n + \mathbf{U}_{i,j+1}^n)$$

The coefficients  $\alpha_i$  are chosen to obtain a fourth-order accuracy in time when the spatial operator is linear.<sup>11</sup> In this case, the stability limit corresponds to a Courant-Friedrichs-Lewy (CFL) number less than 1.73, and the accuracy limit is  $\text{CFL} < 0.73$ . Two other time-integration schemes have been investigated<sup>15</sup> in the case of a nonlinear propagation, but the differences between these time schemes are too small to be noticed.

### 2.3 Boundary Conditions

The boundary conditions are very important in computational aeroacoustics<sup>1</sup> (CAA). Indeed, because of the high quality of the solution, any disturbance of small amplitude can propagate in the computational domain contaminating the numerical solution. The boundary conditions of Tam and his colleagues<sup>9,12</sup> are implemented. The radiation boundary condition for outgoing acoustic waves is based on an asymptotic solution of the linearized Euler's equations. In polar coordinates  $(r, \theta)$ , we have:

$$\left( \frac{\partial}{\partial t} + V(\theta) \frac{\partial}{\partial r} + \frac{V(\theta)}{2r} \right) \mathbf{U} = 0$$

when  $r \rightarrow \infty$ .  $V$  is the group velocity of wave propagation in the radial direction defined by:

$$V = \mathbf{u}_o \cdot \mathbf{e}_r + \sqrt{c_o^2 - (\mathbf{u}_o \cdot \mathbf{e}_\theta)^2}$$

For an outflow boundary condition, the pressure disturbance is an acoustic fluctuation, which is not the case for the velocity and density disturbances. For these last two variables, Euler's equations are used.<sup>9</sup> This yields the following set of compatible first-order differential equations:

$$\begin{aligned} \frac{\partial \rho'}{\partial t} + \mathbf{u}_o \cdot \nabla \rho' &= \frac{\partial p'}{\partial t} + \mathbf{u}_o \cdot \nabla p' \\ \frac{\partial u'}{\partial t} + \mathbf{u}_o \cdot \nabla u' &= -\frac{1}{\rho_o} \frac{\partial p'}{\partial x} \\ \frac{\partial v'}{\partial t} + \mathbf{u}_o \cdot \nabla v' &= -\frac{1}{\rho_o} \frac{\partial p'}{\partial y} \\ \frac{\partial p'}{\partial t} + V(\theta) \left\{ \cos \theta \frac{\partial p'}{\partial x} + \sin \theta \frac{\partial p'}{\partial y} + \frac{p'}{2r} \right\} &= 0 \end{aligned}$$

### 3. Source radiation in a uniform mean flow

Several test problems can be found in the literature to evaluate numerical algorithms in CAA.<sup>13,14</sup> Some

problems have been investigated<sup>15</sup> with the numerical algorithm (3). This section deals with the radiation of a source in a subsonic and a supersonic mean flow. The analytic solution is known for these two problems. The source is implemented by using the vector  $\mathbf{S}$  in the system (2), which yields:

$$\mathbf{S}(x, y, t) = \epsilon \sin \omega t e^{-\alpha(x^2+y^2)} \begin{pmatrix} 1 \\ 0 \\ 0 \\ 1 \end{pmatrix} \quad (4)$$

with  $\alpha = \ln 2/2$ . This value corresponds to the smallest size of a source in order to perform a calculation without damping, i.e.  $R_s = \infty$ , in the subsonic case. The amplitude is taken as  $\epsilon = 0.5$  and the angular frequency is  $\omega = 2\pi/30$ . The time step is given by the condition  $\Delta t = 1/(1+M)$ , corresponding to a CFL number of  $\sqrt{2}$  given that:

$$\text{CFL} = \frac{\Delta t (1+M)}{\Delta r}$$

where  $M$  is the Mach number of the mean flow and  $\Delta r^2 = \Delta x^2 + \Delta y^2$ . The source is located at  $x_s = y_s = 0$  over the computational domain  $-200 \leq x, y \leq 200$ , yielding a regular mesh of  $400 \times 400$  points. Figure 1 displays the time evolution of pressure iso-contours for a subsonic mean flow at  $M = 0.5$ . The pressure profile along the axis  $y = 0$  is plotted in Figure 2, and is compared to the analytical solution obtained by a convolution product of the source term with the 2-D Green function. The two acoustic waves propagate upstream and downstream at the velocity  $1 \pm M$  with an apparent wavelength  $\lambda_c = (1 \pm M) \lambda$  where  $\lambda = 30$ .

The supersonic case is also investigated. The calculation can be performed without filtering but the selective damping with  $R_s = 5$  allows the removal of small oscillations at the limits of the computational domain. Indeed, there is a discontinuity of the boundary conditions due to the Mach cone defined by  $M \sin \theta = 1$ . Figure 3 shows the pressure iso-contours for the case  $M = 1.5$ . The radiated field is very different with respect to the subsonic case. The two acoustic waves propagate now in the downstream direction at the velocity  $M \pm 1$  and interfere with one another. For the value  $M = 1.5$ , the angle of the Mach cone is in the right-hand corners of the domain since the Mach angle is  $\theta \approx 41.8^\circ$ .

The pressure profile along the axis  $y = 0$  is plotted in Figure 4, and is compared to the analytical solution obtained by a convolution product.

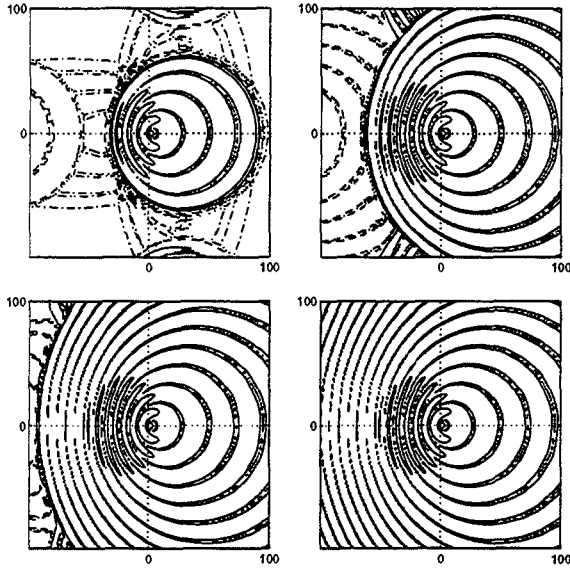


Figure 1: Harmonic source in a uniform subsonic flow at  $M = 0.5$ . Pressure iso-contours every  $t = 45\Delta t$ . —  $10^{-1}$ ,  $10^{-2}$ ,  $10^{-3}$ , - - - -  $10^{-4}$  and - - - -  $10^{-5}$ .

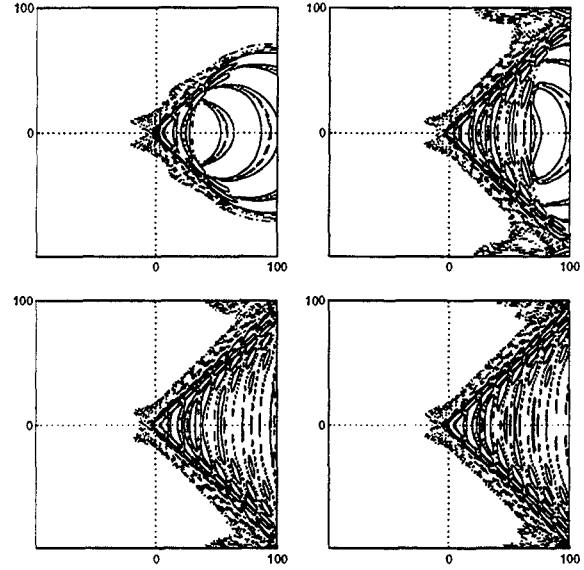


Figure 3: Harmonic source in a uniform supersonic flow at  $M = 1.5$ . Pressure iso-contours every  $t = 80\Delta t$ . —  $10^{-1}$ ,  $10^{-2}$  - - - -  $10^{-3}$  and - - - -  $10^{-4}$ .

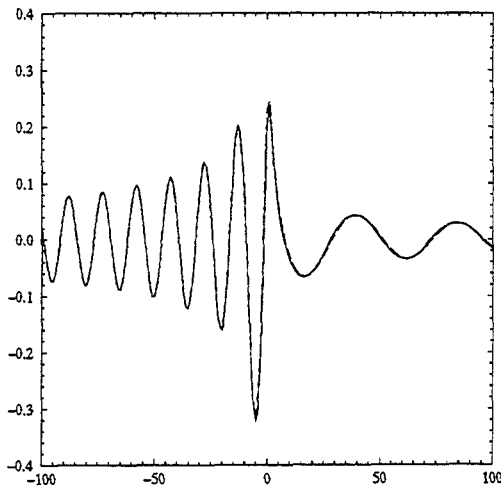


Figure 2: Harmonic source in a uniform subsonic flow at  $M = 0.5$ . Pressure profile along the axis  $y = 0$  at time  $t = 450$ . — numerical solution, - - - - analytical solution.

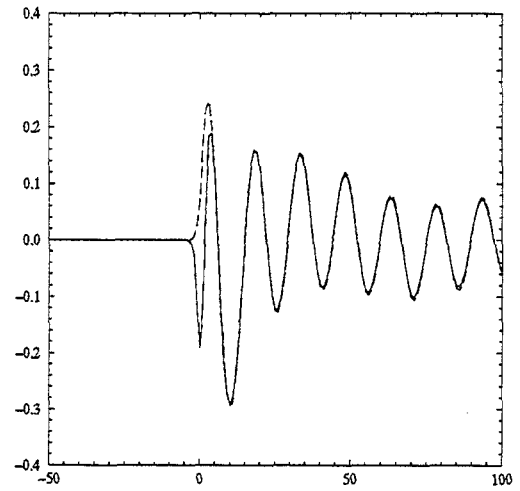


Figure 4: Harmonic source in a uniform supersonic flow at  $M = 1.5$ . Pressure profile along the axis  $y = 0$  at time  $t = 288$ . — numerical solution, - - - - analytical solution.

#### 4. Source radiation in a sheared mean flow

Refraction effects strongly modify the directivity pattern of a source. As an example we consider the radiation of a source placed on the axis of a fully developed jet modeled by a Bickley profile:

$$\frac{u_o}{c_o} = \frac{0.5}{\cosh^2 [(1 + \sqrt{2}) y/b]} \quad (5)$$

The half-width  $b$  of the jet is taken as  $b = 10$ . The source term is given by expression (4). The width of the source is  $\alpha = \ln 2/9$ , the amplitude is  $\epsilon = 0.01$  and the angular frequency is  $\omega = 2\pi/9$ . The wavelength of the source is of the same order of magnitude as the half-width of the jet producing strong refraction effects. This corresponds to a high frequency radiation since the Strouhal number based on the jet diameter  $D = 2b$  and the velocity  $u_o = 0.5c_o$  is  $St = 4.4$ . The same computational domain is used, but the source is now located at  $x_s = -100$  and  $y_s = 0$ . The calculation is performed with a CFL number of  $\sqrt{2}$  and without the artificial selective damping, i.e.  $R_s = \infty$ . Figure 5 shows the pressure field iso-contours. The radiation pattern is strongly modified by the sheared mean flow (5). The acoustic intensity reaches a peak in the downstream direction near the angle  $\theta$  given by the relation  $\cos \theta = 1/(1 + M)$ . For smaller angles, the intensity decreases, and a shadow zone is observed. In the upstream direction, acoustic waves are confined in the jet flow. These results are in agreement with the geometrical approximation valid for high frequencies. Indeed, the ray tracing equations<sup>16</sup> can be solved to obtain a reference solution:

$$\begin{cases} \frac{dx_i}{dt} = c_o \frac{k_i}{k} + u_{oi} \\ \frac{dk_i}{dt} = -k_j \frac{\partial u_{oj}}{\partial x_i} \end{cases}$$

These differential equations are integrated in time with the following initial conditions at  $t = 0$ :  $\mathbf{x} = \mathbf{x}_s$ , and:

$$\mathbf{k} = \frac{k_o}{1 + \nu \cdot \mathbf{M}} \begin{pmatrix} \cos \theta \\ \sin \theta \end{pmatrix}$$

where  $\nu = \mathbf{k}/k$  is the unit vector normal to the wave front,  $k_o = \omega/c_o$  and  $\mathbf{M} = \mathbf{u}_o/c_o$ . The ray tracing is displayed in Figure 6 showing that the radiation features are well illustrated, and the waves fronts have the same characteristic oval pattern. The final time calculation corresponding to Figure 5 is 90 times the time of the source cycle, and the wavelength is  $\lambda = 9$ .

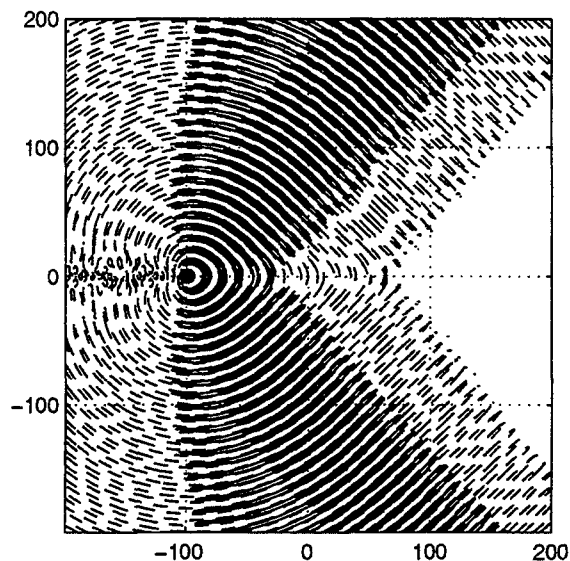


Figure 5: Radiation of a source point in a sheared mean flow. Instantaneous pressure contours at time  $t = 800$ . — isolines from 0.001 to 0.02 (increment 0.001), - - - - isoline  $10^{-4}$ .

Thus, this example shows the steady behavior of the numerical algorithm (3).

It is well known that three modes are supported by the linearized Euler's equations, namely the acoustic waves, the entropy wave and the vorticity wave. However the instability modes of the Bickley jet (5) can not develop with the chosen value of the source frequency. The amplification rate is plotted in Figure 7 as a function of the angular frequency. The nondimensionalized frequency is too high in our case since  $\omega b/u_o \approx 14$ . This point will be discussed in section 6 which is devoted to a nonlinear formulation of the system (2).

#### 5. Definition of a multipolar source

The multipolar feature of a source  $\mathbf{S}$  in the system (2) is clearly identified by writing the wave equation corresponding to the linearized Euler's equations. The linearized Euler's equations take the simplified form:

$$\begin{cases} \frac{\partial \rho'}{\partial t} + \rho_o \frac{\partial u'_i}{\partial x_i} = 0 \\ \rho_o \frac{\partial u'_i}{\partial t} + \frac{\partial p'}{\partial x_i} = S_i \end{cases} \quad (6)$$

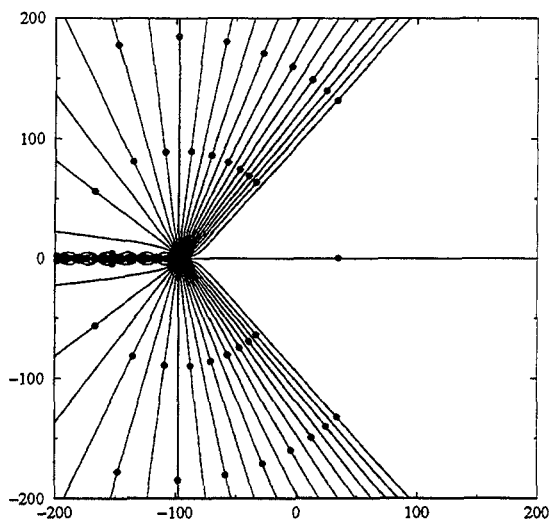


Figure 6: Ray tracing for the radiation of a point source in a sheared mean flow (5). The angle of the shadow zone given by  $\cos \theta = 1/(1 + M)$ , which gives  $\theta \approx 48^\circ$  is well illustrated. The wave fronts are marked by the symbols  $\bullet$ .

for an homogeneous medium at rest, and the associated wave equation is:

$$\frac{\partial^2 \rho'}{\partial t^2} - c_0^2 \nabla^2 \rho' = -\nabla \cdot \mathbf{S} \quad (7)$$

Thus, a dipole distribution  $S_i = F_i$  in the wave equation (7) is defined by:

$$\int_V \frac{\partial F_i}{\partial x_i} dx = \int_S n_i F_i dS = 0$$

with:

$$\int_V F_i dx \neq 0$$

whereas a quadrupole distribution  $S_i = \partial T_{ij} / \partial x_j$  is defined as:

$$\int_V \frac{\partial^2 T_{ij}}{\partial x_i \partial x_j} dx = 0 \quad \text{and} \quad \int_V \frac{\partial T_{ij}}{\partial x_j} dx = 0$$

With regard to aerodynamic noise applications, it is important to check that the resolution of linearized Euler's equations preserves the multipolar feature of the sources. Therefore, a dipole distribution  $F_i$  is investigated, given by:

$$F_1 = \epsilon \cos\left(\frac{\pi}{10}x\right) e^{-\alpha y^2} \sin(\omega t) \quad \text{and} \quad F_2 = 0$$

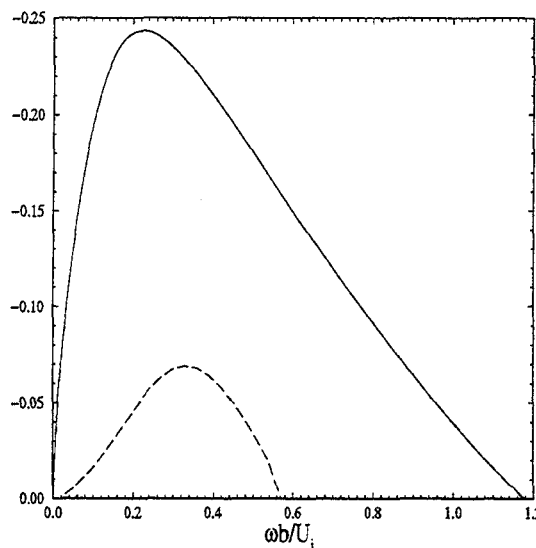


Figure 7: Bickley jet profile (5). Spatial growth rate  $-k_i b$  as a function of the frequency  $\omega b / u_0$ . The velocity perturbation is described by the stream function  $\Psi(x, y) = \phi(y) e^{ik(x-ct)}$ , where the wave number  $k \in \mathbb{C}$  and the wave speed  $c \in \mathbb{C}$ . — sinusoidal mode, - - - - varicose mode.

where  $(x, y) \in [-5; 5] \times \mathbb{R}$ . A quadrupole distribution  $T_{ij}$  in system (6), is defined such that:

$$T_{ij} = \begin{bmatrix} -\cos\left(\frac{\pi}{20}x\right) e^{-\alpha y^2} & 0 \\ 0 & \cos\left(\frac{\pi}{20}y\right) e^{-\alpha x^2} \end{bmatrix} \times \frac{20}{\pi} \epsilon \sin(\omega t)$$

in  $(x, y) \in [-10; 10] \times [-10; 10]$ . The angular frequency is taken as  $\omega = 2\pi/60$ , the amplitude of the source is  $\epsilon = 0.01$  and the coefficient  $\alpha$  is equal to  $(\ln 2)/5$ . Figure 8 shows the density iso-contours: the dipole directivity is well illustrated.

For the dipole distribution, the wave equation (7) can be written as:

$$\frac{\partial^2 \rho'}{\partial t^2} - c_0^2 \nabla^2 \rho' = -\nabla \cdot \mathbf{F}$$

when spatial derivatives of the source term (6) appear. Therefore, this problem is difficult for noise generation<sup>17</sup> since the size of the source domain has the same order of magnitude as wavelength. A comparison between the calculated density profile along the axis  $y = 0$  and the analytical solution is plotted in Figure 9 for two points in time. The exact

solution is given by the convolution product  $\rho' = -F_1 * \partial G / \partial x$  where the Green function is given by:

$$G(\mathbf{x}, t) = \left[ \frac{i}{4c_o^2} H_o^{(1)} \left( \frac{\omega}{c_o} r \right) e^{-i\omega t} \right] \quad (8)$$

with  $\mathbf{x} = (x, y)$ ,  $r = \sqrt{x^2 + y^2}$  and  $H_o^{(1)}$  designates the Hankel function of order zero. The acoustic field is calculated very accurately, without spurious oscillations near the source domain. For these computations, the mesh Reynolds number of the damping is  $R_s = 5$ . For the quadrupole distribution, the radiated field is governed by the following wave equation:

$$\frac{\partial^2 \rho'}{\partial t^2} - c_o^2 \nabla^2 \rho' = -\nabla \cdot (\nabla \cdot \mathbf{T})$$

Figure 10 displays the acoustic field radiated by the quadrupole distribution where the expected directivity is again well shown. The analytical solution takes the form of a sum of two convolution products:

$$\rho' = -\frac{\partial T_{xx}}{\partial x} * \frac{\partial G}{\partial x} - \frac{\partial T_{yy}}{\partial y} * \frac{\partial G}{\partial y}$$

where the Green function is given by expression (8). Two comparisons between computations and the exact solution are shown in Figure 11. Unlike the dipole distribution, small oscillations near the source are present. Indeed, in the quadrupole distribution, the source term in the system (6) is not zero on the boundaries. A last test has been carried out in setting the source term  $S_i = \partial T_{ij} / \partial x_j$  in the jet profile (5). The half-width is taken as  $b = 20$  and the center of the source domain is  $x_s = -100$  et  $y_s = 0$ . The radiated pressure field (Figure 12) is strongly modified by refraction effects with respect to the no-flow situation. However, the multipolar nature of the source is again clearly identifiable.

## 6. Nonlinear propagation

A nonlinear formulation has been developed in order to saturate the growth of instability waves. The linear propagation governing by equations (2) becomes:

$$\frac{\partial \mathbf{U}}{\partial t} + \frac{\partial \mathbf{E}}{\partial x} + \frac{\partial \mathbf{F}}{\partial y} + \frac{\partial \mathbf{E}_{nl}}{\partial x} + \frac{\partial \mathbf{F}_{nl}}{\partial y} + \mathbf{H} = \mathbf{S} \quad (9)$$

where the flux vectors containing all the nonlinear terms are written as:

$$\mathbf{E}_{nl} = \begin{pmatrix} \rho' u' \\ \rho_o u'^2 + 2\rho' u' u_o + \rho' u'^2 \\ \rho' u' v' + \rho' u' v_o + \rho' v' u_o + \rho_o u' v' \\ \rho' u' \end{pmatrix}$$

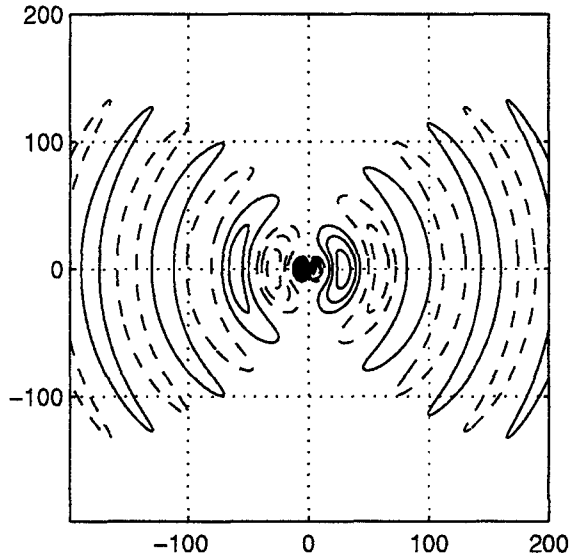


Figure 8: Dipole distribution  $S_i = F_i$ . Density isocontours at time  $t = 640\Delta t$ . — positive values, from 0.001 to 0.011 with a step size of 0.001, ----- negative values.

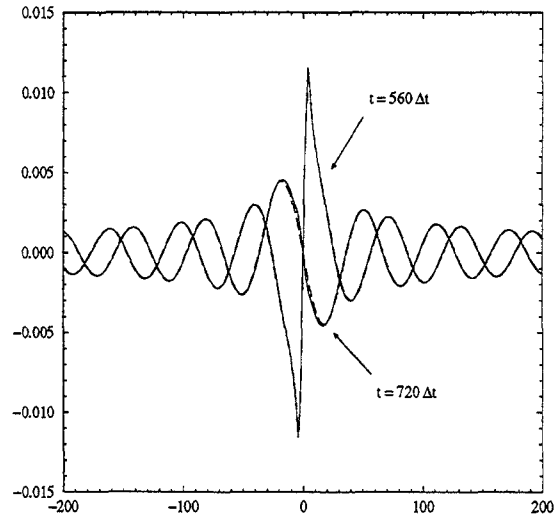


Figure 9: Dipole distribution  $S_i = F_i$ . Two density profiles along the axis  $x_2 = 0$  at times  $t = 560\Delta t$  and  $t = 720\Delta t$ . — numerical solution, ----- analytical solution.

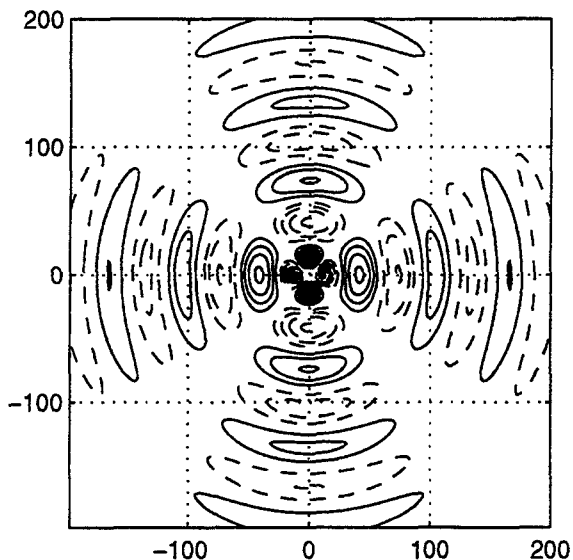


Figure 10: Quadrupole distribution  $S_i = \partial T_{ij} / \partial x_j$ . Density iso-contours at time  $t = 640\Delta t$ . — positive values, from 0.001 to 0.011 with a step size of 0.001, - - - - negative values.

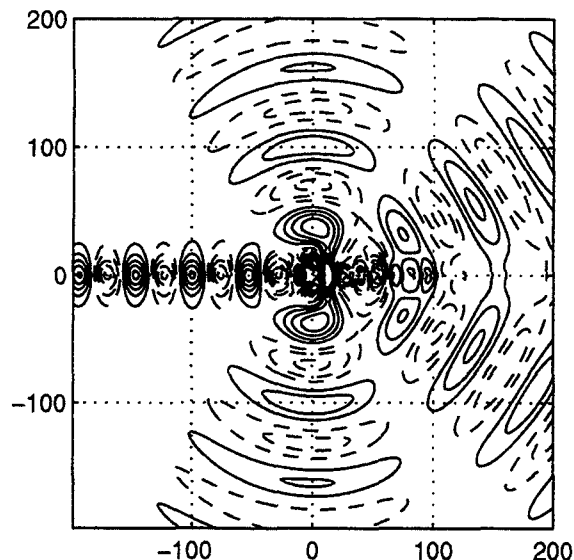


Figure 12: Quadrupole distribution  $S_i = \partial T_{ij} / \partial x_j$  in the jet profile (5) at  $M = 0.5$ . Pressure iso-contours at time  $t = 640\Delta t$ . — positive values, from 0.001 to 0.011 with a step size of 0.001, - - - - negative values.

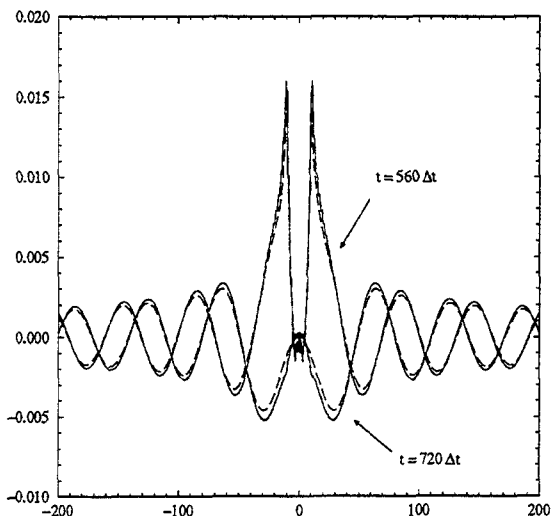


Figure 11: Quadrupole distribution  $S_i = \partial T_{ij} / \partial x_j$ . Two density profiles along the axis  $x_2 = 0$  at times  $t = 560\Delta t$  and  $t = 720\Delta t$ . — numerical solution, - - - - analytical solution.

and

$$F_{nl} = \begin{pmatrix} \rho'v' \\ \rho'u'v' + \rho'u'v_o + \rho'v'u_o + \rho_o u'v' \\ \rho_o v'^2 + 2\rho'v'v_o + \rho'v'^2 \\ p'v' \end{pmatrix}$$

This kind of formulation has been used by Viswanathan & Sankar<sup>18</sup> and Morris<sup>19</sup> *et al.*. The influence of nonlinear terms can be illustrated by the following example. If we assume that the perturbation velocity has the form:

$$\psi(x, y, t) = \phi(y) e^{ik(x-ct)} \text{ with } (k, c) \in \mathbb{C},$$

then the square of the perturbation amplitude  $A = \psi\psi^*$  satisfies the equation:

$$\frac{\partial A}{\partial t} = 2kc_i A \quad (10)$$

where  $c = c_r + ic_i$ . Perturbations are unstable if the imaginary part of the speed  $c$  is positive, i.e.  $c_i > 0$ . In order to include nonlinear effects, the equation (10) is now replaced by:

$$\frac{\partial A}{\partial t} = 2kc_i A - bA^2$$

where  $b$  is a constant. The perturbation amplitude is then given by the expression:

$$\frac{1}{A} = \frac{b}{2kc_i} + \beta e^{-i2kc_it}$$

where  $\beta$  is an integration constant. Thus, the growth of the velocity perturbation is limited by taking into account nonlinear terms.

A symmetric hyperbolic tangent velocity profile given by:

$$u_o = \frac{1}{2} \left[ 1 + \tanh \left( \frac{y+H}{2\delta_\theta} \right) \right] \quad y \geq 0 \quad (11)$$

where the parameters  $H$  and  $\delta_\theta$  are taken as  $H = 9$  and  $\delta_\theta = 1$  is used as mean flowfield in order to observe development of instability waves. The equations (9) are solved with the numerical algorithm given in (3). The mesh Reynolds number is  $R_s = 5$  and the CFL number is taken as  $\sqrt{2}$ . The description of the computational domain and the source term are identical to those provided in section 4.

Figure 13 displays the pressure profile along the axis  $y = 0$ . By solving the nonlinear system (9) the growth of the instability waves is limited. The time evolution of the pressure profiles shows the wave front deformation by nonlinear effects. It is to be noticed that the nonlinear formulation does not change significantly the radiated pressure field. The radial pressure profile along the line  $x = x_s$  is plotted in Figure (14) for the linear and nonlinear calculations. The difference between the two pressure fields is given in the same figure. The relative variation does not exceed 1%.

## 7. Concluding remarks

Computation sound propagation by solving the linearized Euler's equations provides accurate solutions with very good performances in terms of stability, low storage and computation time. The multipolar nature of the source is preserved by the numerical scheme, a crucial point for aerodynamic noise predictions. The growth of instability waves which are supported by linearized's Euler equations, can be limited by taking into account nonlinear terms without altering the evaluation of sound waves. All the results presented in this paper has been obtained in a 2D geometry. An extension of this work to 3D is under development to compute the noise radiated by a subsonic jet.

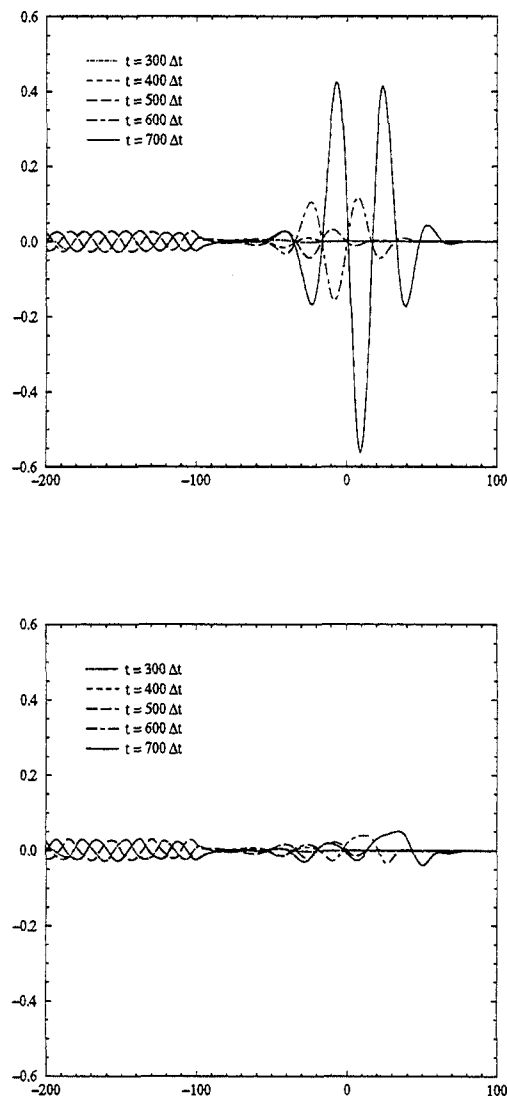


Figure 13: Influence of the nonlinear terms. Pressure profile along the axis  $y = 0$  at different points in time. The upper plot is obtained without the nonlinear terms in solving equations (2). The lower plot is obtained with the nonlinear terms in solving equations (9).

### Acknowledgments

Computing time was provided by Institut du Développement et des Ressources en Informatique Scientifique (IDRIS - CNRS). A part of this work was also supported by the Centre National des Etudes Spatiales (CNES).

### References

- <sup>1</sup>TAM, C.K.W., 1995, Computational aeroacoustics: issues and methods, *AIAA Journal*, **33**(10), 1788-1796.
- <sup>2</sup>LELE, S.K., 1997, Computational Aeroacoustics: a review, *35th Aerospace Sciences Meeting & Exhibit*, AIAA paper 97-0018.
- <sup>3</sup>LIGHTHILL, M.J., 1952, On sound generated aerodynamically - I. General theory, *Proc. Roy. Soc. London*, **211**, A 1107, 564-587.
- <sup>4</sup>VAN HERPE, F., LAFON, P. & CRIGHTON, D., 1995, Noise generation by turbulent flow in a duct obstructed by a diaphragm, AIAA paper 95-035.
- <sup>5</sup>BÉCHARA, W., BAILLY, C., LAFON, P. & CANDEL, S., 1994, Stochastic approach to noise modeling for free turbulent flows, *AIAA Journal*, **32**(3), 455-463.
- <sup>6</sup>BAILLY, C., LAFON, P. & CANDEL, S., 1995, A stochastic approach to compute noise generation and radiation of free turbulent flows, AIAA Paper 95-092.
- <sup>7</sup>BAILLY, C., LAFON, P. & CANDEL, S., 1996, Computation of noise generation and propagation for free and confined turbulent flows, AIAA Paper 96-1732.
- <sup>8</sup>GRÈVERIE, L. & BAILLY, C., 1998, Reconstruction d'un opérateur de propagation à partir des équations d'Euler linéarisées, submitted to the *Comptes Rendus de l'Académie des Sciences, Paris*.
- <sup>9</sup>TAM, C.K.W. & WEBB, J.C., 1993, Dispersion-relation-preserving finite difference schemes for computational acoustics, *J. Comput. Phys.*, **107**, 262-281.
- <sup>10</sup>TAM, C.K.W. & SHEN, H., 1993, Direct computation of nonlinear acoustic pulses using high order finite difference schemes, AIAA Paper 93-4325.

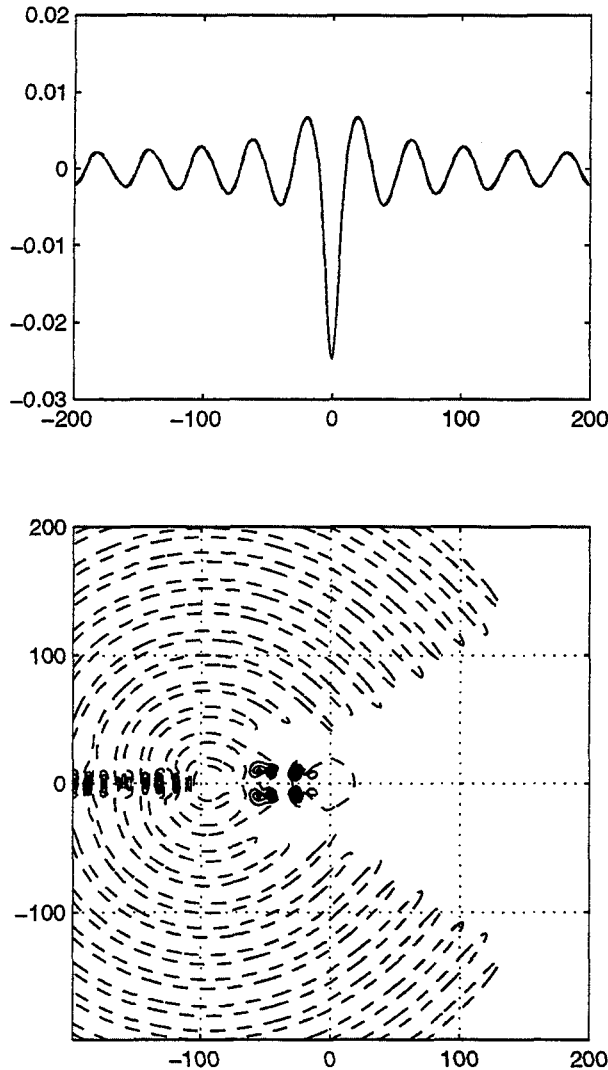


Figure 14: Nonlinear formulation. The upper plot shows a comparison of the radial pressure profile along the line  $x = x_s$  at time  $t = 800\Delta t$ : — with nonlinear terms, ---- without nonlinear terms. The lower plot shows the perturbation pressure isocontours obtained by taking the difference between the two formulations. The radiated acoustic field is not modified by taking into account nonlinear terms. — from 0.001 to 0.02 with a step size of 0.001, --  $10^{-4}$ .

- <sup>11</sup>HU, F.Q., HUSSAINI, M.Y. & MANTHEY, J.L., 1996, Low-dissipation and low-dispersion Runge-Kutta schemes for computational acoustics, *J. Comput. Phys.*, **124**, 177-191.
- <sup>12</sup>TAM, C.K.W. & DONG, Z., 1995, Radiation and outflow boundary conditions for direct computation of acoustic and flow disturbances in a nonuniform mean flow, AIAA Paper 95-007.
- <sup>13</sup>ICASE / NASA, 1995, Workshop on benchmark problems in computational aeroacoustics, NASA CP 3300, edited by Hardin, J.C., Ristorcelli, J.R. & Tam, C.K.W.
- <sup>14</sup>ICASE / NASA, 1997, Second computational aeroacoustics workshop on benchmark problems NASA CP 3352, edited by Tam, C.K.W. & Hardin, J.C.
- <sup>15</sup>BAILLY, C., THÉVENIN, R. & JUVÉ, D., 1997, Numerical simulation of sound source radiation in flows, *Third International Conference on Theoretical & Computational Acoustics*, Newark, New Jersey, USA, July 14-18.
- <sup>16</sup>CANDEL, S.M., 1977, Numerical solution of conservation equations arising in linear wave theory: application to aeroacoustics, *J. Fluid Mech.*, **83**(3), 465-493.
- <sup>17</sup>CRIGHTON, D., 1975, Basic principles of aerodynamic noise generation, *Prog. Aerospace Sci.*, **16**(1), 31-96.
- <sup>18</sup>VISWANATHAN, K. & SANKAR, L.N., 1995, Toward the direct calculation of noise: fluid/acoustic coupled simulation, *AIAA Journal*, **33**(12), 2271-2279.
- <sup>19</sup>MORRIS, P.J., WANG, Q., LONG, L.N., LOCKARD, D.P., 1997, Numerical predictions of high speed jet noise, AIAA Paper 98-1598.